LANGMUIR

pubs.acs.org/Langmuir Article

Collective Oscillations of Photothermal Micromotors under Static Illumination

Dan Wang,* Yuhang Zhang, Mingtong Li, Youyi Xia, Ling Jin, BingBing Wang, Hong Gao, Mingcheng Yang,* and Bin Dong*

Cite This: *Langmuir* 2026, 42, 21207−21216 Read Online

ACCESS | Metrics & More | Article Recommendations | Supporting Information

ABSTRACT: Nonlinear phenomenon widely exists in living organisms in nature. Over the past decades, self-propelled micromotors with oscillatory behaviors have aroused focus of attentions. However, oscillatory behaviors driven by nonchemical mechanisms have rarely been explored. In this paper, we report a collective oscillation of photothermal micromotors driven by the periodic variation of a photothermally induced temperature difference, which leads to an alternating two-mode motion, a slow mode driven by the synergistic effects of self-thermophoresis and thermocapillary forces (∼70 μm/s) and a fast mode driven by thermal convection (∼2422 μm/s). The oscillatory behavior is tunable by adjusting the light intensity and the concentration of microspheres. The present findings not only provide fresh insight into emergent collective behaviors of active matter but also pave the way toward the study of more complex and coupled oscillatory active systems.

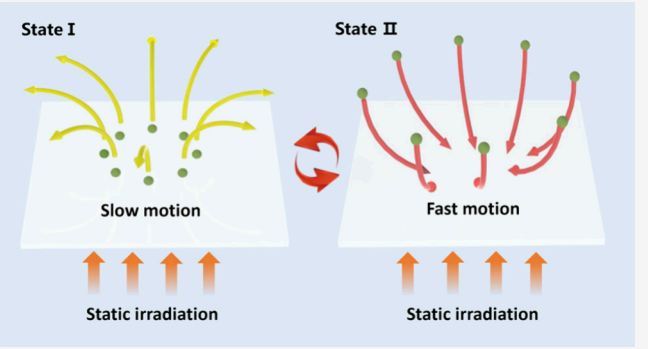

INTRODUCTION

Nonlinear behavior is a ubiquitous phenomenon in nature. From cardiac pulsation and neuronal firing to biological rhythms, nonlinear dynamics play a crucial role across various scales in the natural world.[1−3] Inspired by such dynamics in nature, researchers have begun to artificially design self-propelled systems that exhibit similar nonlinear behaviors. Synthetic self-propelled motors are a kind of smart devices capable of converting external energy (e.g., light,[4−8] magnetic field,[9−11] electric field,[12−14] ultrasound,[15,16] and chemical fuels[17−19]) into kinetic energy, thereby achieving autonomous movement. Recently, self-propelled motors with nonlinear oscillatory behavior, which have been investigated across multiple scales, have aroused focus of attentions. At the centimeter or millimeter scale, bubble-propulsion[20] or Marangoni effect-driven motors[21−23] can exhibit macroscopic oscillations in moving velocity at air−liquid interfaces, while at the micro/nano scale, colloidal particles based on self-diffusiophores[24−26] or electroosmotic flow[27] can also display periodic velocity or morphological oscillations.

Among these different types of oscillatory behaviors, collective oscillations of colloidal particles not only rely on the self-propulsion capability of individual particles but also require synergistic interactions among particles, especially the synchronized oscillations in spatial distribution, morphology, or size.[28] However, most reported oscillatory systems are based on nonlinear chemical reactions, such as those analogous to Belousov−Zhabotinsky (BZ) reactions.[29] Therefore, exploring collective oscillations driven by nonchemical mechanisms is of great significance for expanding the functionality and applications of active colloidal systems. The local temperature gradients generated by the photothermal effect in a fuel-free manner have been widely used to power micromotors via self-thermophoresis.[23,30−32] While photothermal effect has also been exploited to drive the migration of macroscopic oil droplets on aqueous surfaces via the thermal Marangoni effect.[33] Since a steady temperature gradient cannot oscillate on its own, photothermal micromotors that show collective oscillations with a two-mode switch have not been reported yet. It is therefore desirable to exploit such oscillatory collective behaviors in photothermal micromotors, which would provide new avenues for active colloids and autonomous microsystems.

Herein, we report a unique oscillatory collective behavior of photothermal poly(vinyl alcohol)-polypyrrole (PVA−PPy)-based micromotors under static illumination. The PVA−PPy micromotors are synthesized by a one-step emulsion method and are capable of converting light into heat. Under

Received: April 11, 2026
Revised: July 3, 2026
Accepted: July 5, 2026
Published: July 14, 2026

https://doi.org/10.1021/acs.langmuir.6c02095
Langmuir 2026, 42, 21207−21216

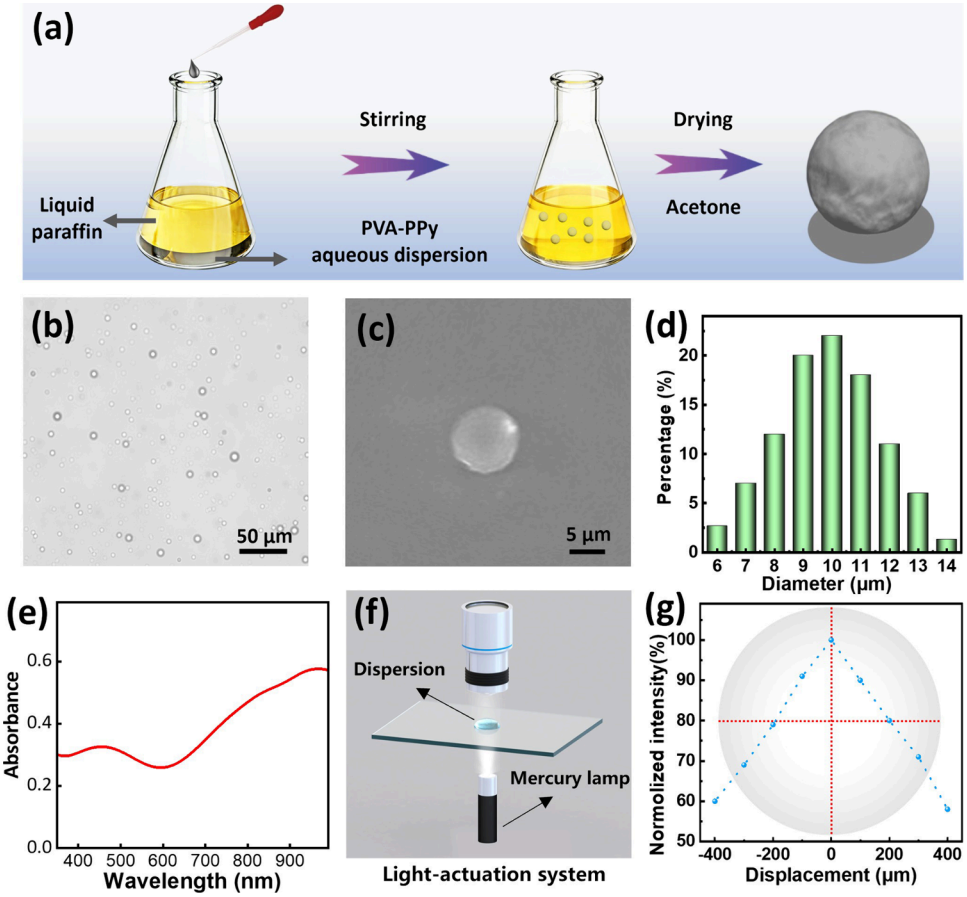

Figure 1. Preparation and Characterization of PVA−PPy microspheres. (a) Schematic illustration showing one-step fabrication process of PVA−PPy microspheres using the water-in-oil emulsion method. (b) Optical microscope image and (c) SEM image of PVA−PPy microsphere. (d) Size distribution histogram of the PVA−PPy microspheres' diameter. (e) UV-vis-NIR absorption spectrum of PVA−PPy microsphere. (f) Schematic illustration showing the construction of a light-actuation system. (g) The distribution of light intensity versus displacement from the position to the center of the light spot.

illumination, these microparticles exhibit collective oscillatory behavior characterized by the switching between two distinct motion modes. The particles initially undergo slow movement driven by thermophoresis/thermocapillary flow, followed by rapid motion propelled by thermal convection. The system periodically alternates between these two modes, with the motion pattern and speed continually switching back and forth. The oscillation frequency can be modulated by the light intensity and the concentration of the micromotors. Moreover, this oscillation occurs within a certain range of light intensity and motor concentration. While beyond this range, the motion becomes single-mode. This phenomenon could stimulate the development of new collective behavior for the artificial micromotors.

RESULTS AND DISCUSSION

Fabrication and Characterization of PVA−PPy Micromotors

PVA−PPy micromotors were fabricated via a one-step water-in-oil (liquid paraffin in water) emulsion method, as illustrated in Figure 1a. This emulsion method allows large-scale production of micromotors, which is especially useful for studying collective behaviors that require high particle densities. The resulting PVA−PPy microparticles exhibit a uniform spherical morphology, as confirmed by both optical microscopy and scanning electron microscopy (SEM) (Figure 1b,c). The size distribution histogram (Figure 1d) reveals an average diameter of approximately 10 μm, with a narrow distribution indicative of good size control during synthesis.

The optical absorption properties of the PVA−PPy microspheres were characterized by UV-vis-NIR spectroscopy. As shown in Figure 1e, the material displays a broad absorption band spanning from 400 to 1000 nm, with two distinct peaks centered at 470 and 970 nm. These characteristic peaks originate from the polypyrrole component, confirming that the PVA−PPy microspheres possess excellent light-absorbing capability and efficient photothermal conversion, which are key for light-driven actuation. The chemical composition of the PVA−PPy microspheres was further analyzed by Fourier transform infrared (FTIR) spectroscopy (Figure S1 in the Supporting Information). Characteristic absorption bands corresponding to polypyrrole were observed at 3407 cm^{-1} (N−H stretching) and 1632 cm^{-1} (C═N/pyrrole ring skeleton vibration). Additionally, bands attributed to poly(vinyl alcohol) were identified at 3407 cm^{-1} (O−H stretching), 2927 cm^{-1} (C−H stretching), and 1086 cm^{-1} (C−O stretching). These results confirm the successful incorporation of both PVA and PPy in the composite microspheres. A schematic diagram of the light-actuation system is presented in Figure 1f. A water droplet (120 μL) containing dispersed PVA−PPy microspheres was placed on a

https://doi.org/10.1021/acs.langmuir.6c02095
Langmuir 2026, 42, 21207−21216

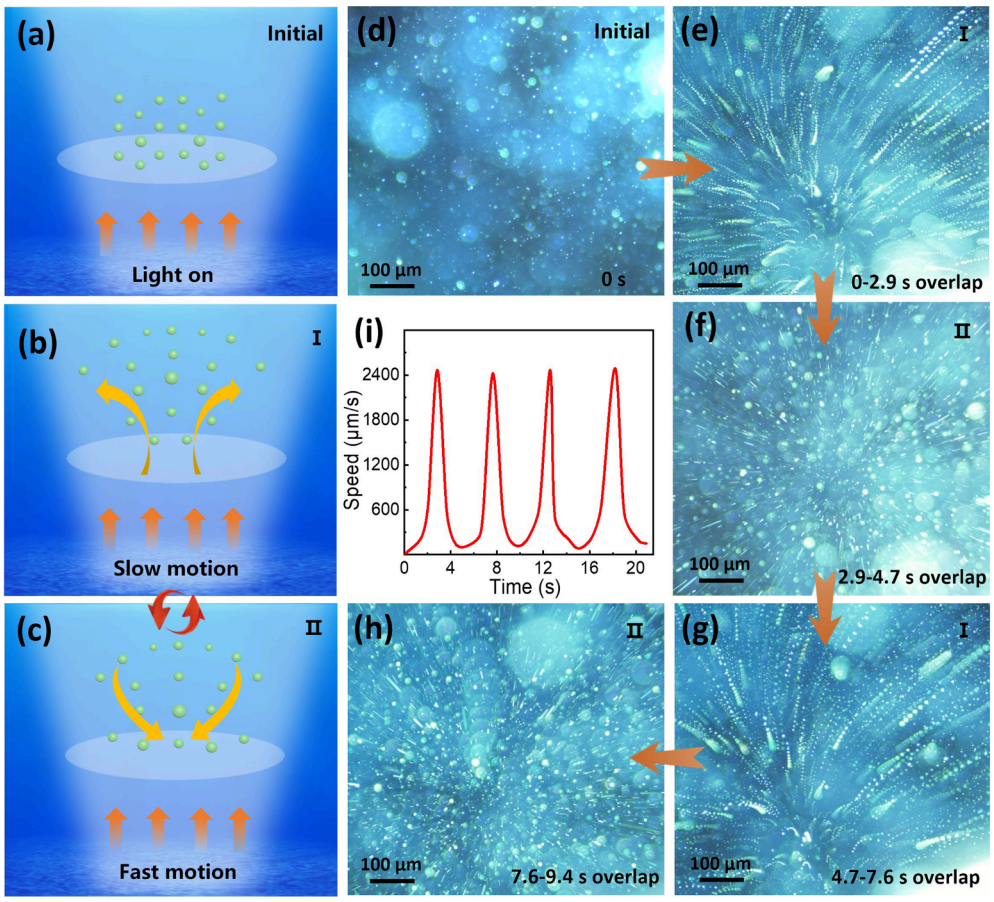

Figure 2. Schematic illustration showing the light-driven oscillatory behavior of PVA−PPy microspheres with different states: (a) Initial state upon light irradiation. (b) Microspheres move upward toward the edge of the droplet at a slow speed. (c) Microspheres move downward toward the center at a fast speed based on high-speed convection. (d−h) A series of CCD images showing the light-driven oscillatory motion of PVA−PPy microspheres in different states. (i) Oscillation of speed of PVA−PPy microspheres versus time when irradiated with 0.8 W/cm^2.

glass slide positioned above a light source, with the entire light-actuation system under a microscope lens for real-time observation. The wetted area observed from above had a diameter of approximately 15 mm (radius ∼ 7.5 mm). The height at the lowest point (the central depression of the thin layer) was approximately 1 mm. The maximum height near the center was approximately 1.3 mm. Moreover, the focal plane was consistently maintained at the middle-to-upper region of the droplet, i.e., well above the midplane but not directly at the top air−water interface. The illumination was applied from below the glass slide, and as shown in Figure 1g, the light intensity exhibited a radial decay from the center to the edge of the light spot, which plays an important role in establishing the temperature gradients in the horizontal and vertical directions.

Light-Driven Oscillatory Behavior of PVA−PPy Micromotors

The PVA−PPy micromotors exhibit unique collective oscillations upon light irradiation, as shown in Figure 2 and Video S1 (Light-driven oscillatory collective behavior of PVA−PPy microspheres) in the Supporting Information. Owing to the close density of PVA−PPy and water, PVA−PPy microspheres can suspend motionlessly in the water droplet without external stimuli, as shown in Figure 2a,d (t = 0 s). Upon light irradiation applied vertically below the solution with a medium intensity of 0.8 W/cm^2, PVA−PPy microspheres (0.4 vol % in water) start to move toward the upper and edge of the region with a slow speed of 70 μm/s (state I), as shown in Figure 2b,i and the overlap image of the microspheres in Figure 2e. The defocus blurring observed in the recorded video further confirms this upward motion. Microspheres initially below the focal plane become clearer as they rise toward it and then blurred as they continue past it toward the top surface, consistent with sustained upward movement. Upon reaching the edge of the droplet, the particles move downward and inward (Figure 2c,f), following the direction of the convective flow with a fast speed of 2422 μm/s (state II), which is much higher than the previous moving speed (Figure 2f,i). During this phase, microspheres move downward away from the top surface, as indicated by the rapid increase in defocus blur when they sink below the focal plane (Figure 2f). Then, the speed of microspheres decreases significantly after reaching the maximum speed, and finally returns to the initial state at t = 4.7 s. After that, another cycle begins, as shown in Figure 2g,h, the second cycle also lasted for 4.7 s. We found that the particles' speed exhibited periodic oscillations during this process (Figure 2i), which are in perfect synchrony with the corresponding motion patterns of the particles.

So far, there are mainly two types of oscillatory behaviors in nano- and micromotors, including oscillation in morphology and oscillation in speed (Table S1 in the Supporting Information). On the one hand, the most typical mechanism involves two competing reactions that induce reversible

https://doi.org/10.1021/acs.langmuir.6c02095
Langmuir 2026, 42, 21207−21216

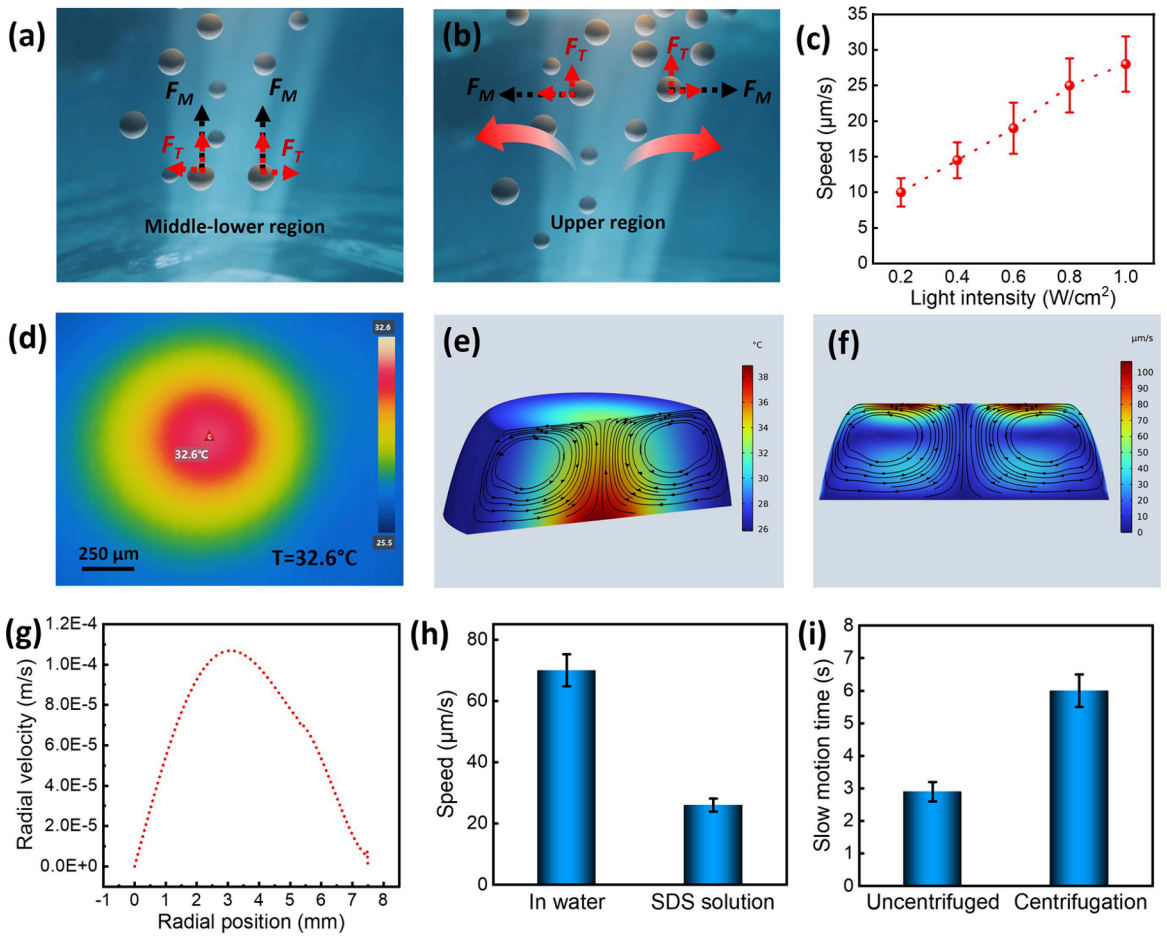

Figure 3. Analysis of the motion mechanism. Schematic illustration showing the propulsion force of microspheres in (a) the middle-lower and (b) upper region. (c) Moving speed of PVA−PPy micromotors under different light intensities. (d) Infrared thermal images showing the liquid droplet containing PVA−PPy microspheres (0.4 vol % in water) with a light intensity of 0.8 W/cm^2. (e) Simulated flow field and temperature distribution of thermal Marangoni flow. (f) Simulated velocity field of thermal Marangoni flow. (g) Simulated radial velocity distribution along the droplet surface. (h) Average moving speed of the slow-motion phase in water and in SDS solution. (i) Moving time of the slow-motion phase in the uncentrifuged and centrifuged dispersion.

changes in the charge distribution around the particles, thereby triggering oscillations in their motion speed or aggregation morphology. These oscillatory behaviors are driven by chemically based principles such as self-diffusiophoresis and electroosmosis. Fuel-free oscillatory mechanisms have rarely been reported. On the other hand, these oscillatory behaviors are primarily observed in two-dimensional planes, while the motion in this work occurs throughout three-dimensional space. Although, a recent study reported photothermal oscillation of hollow microparticles near a droplet surface, but the oscillation relied on a mechanical chopper to periodically modulate the laser, rather than occurring spontaneously under static illumination.[34] Additionally, the overlapped images of particle trajectories reveal that the oscillation shows not only differences in speed but also in the motion mode.

Motion Mechanism of Oscillatory Collective Behavior

Our findings suggest that the movement could be induced by two distinct mechanisms. First of all, we analyzed the propulsion mechanism of the slow-motion phase. When light first irradiates the particles, the particles start to move toward the upper and edge of the region, which may be propelled by thermocapillary flow (also known as thermal Marangoni flow) and self-thermophoresis, as can be seen from Figure 3a,b. Note that as the light intensity decays radially from the center, the particles simultaneously experience a vertical upward thermophoretic force and a horizontal thermophoretic force. The moving speed of slow motion can reach 70 μm/s, which is much greater than the speed limit of self-thermophoresis of a single PVA−PPy microsphere (Figure 3c, 25 μm/s in 0.8 W/cm^2). Therefore, this propulsion is not only powered by self-thermophoresis, but also propelled by other photothermal-induced propulsion forces.

To demonstrate the critical role of thermocapillary force in the slow-motion phase, the particle dispersion containing 0.5 wt % surfactant Sodium Dodecyl Sulfate (SDS) was investigated, which can efficiently reduce the interfacial tension. As shown in Figure 3h, the speed of the particles during the slow-motion phase decreased significantly in the surfactant solution (to less than 30 μm/s). This result provides direct evidence that the upward and outward particle migration is driven by the synergistic effects of self-thermophoretic (F_T) and thermocapillary forces (F_M). Additionally, the infrared thermal images (Figure 3d) of the droplet reveal that the temperature decays gradually from the center outward, leading to the outward Marangoni flow from the center by the temperature gradient. To further verify the domination of

https://doi.org/10.1021/acs.langmuir.6c02095
Langmuir 2026, 42, 21207−21216

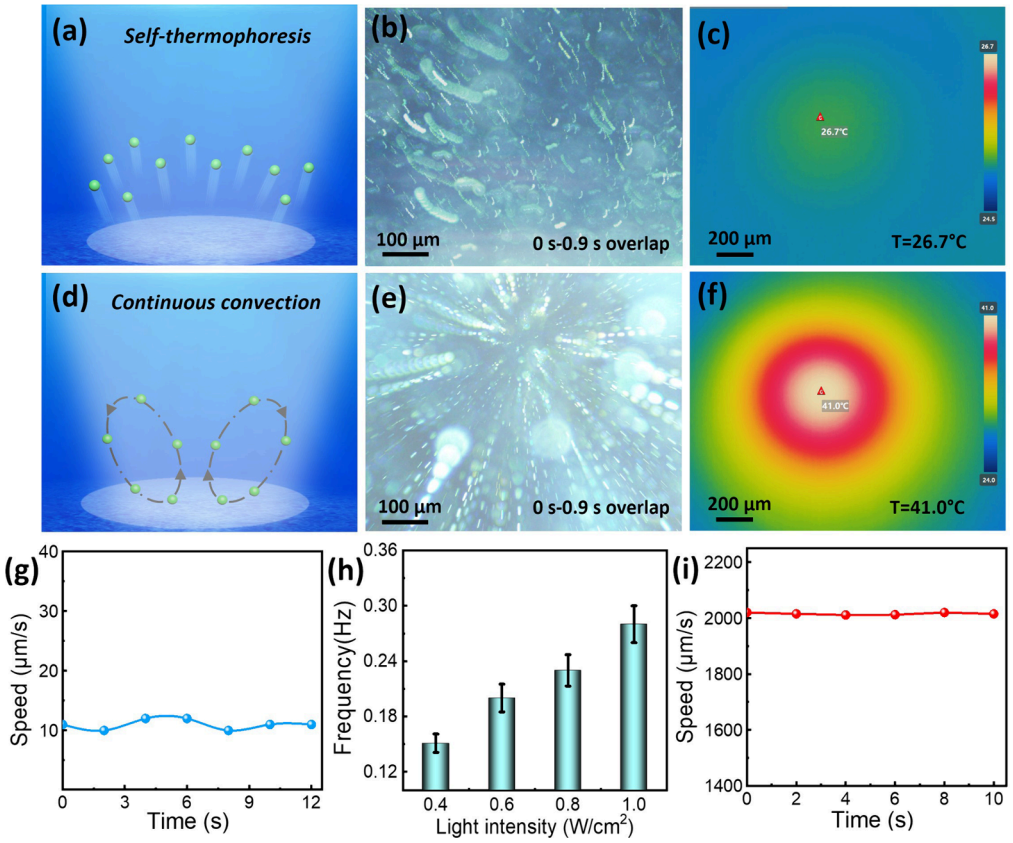

Figure 4. Influence of light intensity. (a) Schematic illustration showing the self-thermophoresis motion of PVA−PPy microspheres (0.4 vol %) upon weak light intensity (0.2 W/cm^2) and (b) corresponding overlaid CCD images, (c) infrared thermal images. (d) Schematic showing the continuous motion of PVA−PPy microspheres upon strong light intensity (1.2 W/cm^2) and (e) corresponding overlaid CCD images, (f) infrared thermal images. (g) Moving speed of PVA−PPy microspheres vs time when irradiated with low light intensity (0.2 W/cm^2). (h) The oscillation frequency of PVA−PPy microspheres under different light intensities. (i) Moving speed of PVA−PPy microspheres vs time when irradiated with high light intensity (1.2 W/cm^2).

Marangoni flow in the slow-motion phase, we performed finite-element simulations using COMSOL Multiphysics (see Section S4 in the Supporting Information for model details). As shown in Figure 3e, the simulated temperature field exhibits a radial decay from the center to the edge, closely matching the experimental infrared image (Figure 3d). Moreover, as observed in the flow field in the vertical direction, the temperature gradually decays upward from the bottom heat source, and the flow direction shifts from nearly vertical in the middle-lower region to outward from the center in the upper region. This is consistent with the particle's trajectory in Figure 2e. The corresponding simulated velocity field (Figure 3f) and radial velocity profile (Figure 3g) reveal a strong outward surface flow (about ∼110 μm/s) driven by the temperature-induced surface tension gradient, which closely matches the speed (∼70 μm/s) measured in the experiment. Therefore, the thermophoretic force (F_T) gradually decreases during the upward motion of micromotors. At the same time, the particles move outward from the center propelled by the strong thermal Marangoni flow (F_M; Figure 3b). Furthermore, the calculation of the Marangoni number is 1109, which further confirms the crucial role of thermal Marangoni flow (for details, please refer to Section S4 in the Supporting Information).

Moreover, the propulsion of the fast-motion phase has been further investigated. Since the fast motion starts suddenly after the slow motion, it clearly requires a threshold to be triggered. Thermal convection is known to possess such a threshold, whereas thermocapillary (Marangoni) flow does not. This suggests that the rapid motion is likely triggered by thermal convection. To further rule out the influence of thermocapillary flow in fast-motion mode, we introduced a dispersion of PVA−PPy micromotors into a glass sandwich, allowing it to fill the entire gap with the thickness of 1 mm, thereby completely eliminating any free liquid−air interface (Figure S2 in the Supporting Information). Under illumination, no thermocapillary flow can be generated in this condition. High-speed motion can still be observed under light irradiation (Figure S3 in the Supporting Information), indicating the rapid motion is induced by thermal convection when the temperature difference exceeds threshold value. Notably, the coupling of thermophoresis and thermal convection has previously been exploited for steady-state microparticle trapping using an external heat source.[35]

This high-speed thermal convection is driven by the vertical temperature difference, making the dispersion state of the particles crucial. As shown in Figure 3i, the time consumed during the slow-motion phase was recorded for both centrifuged and noncentrifuged particles. The results indicate that droplets containing centrifuged particles require approximately twice the time to trigger high-speed convection, demonstrating that particle dispersion during the slow-motion phase facilitates the formation of a vertical temperature difference in reaching the threshold required for thermal convection. As a result, it takes a certain amount of time for the

https://doi.org/10.1021/acs.langmuir.6c02095
Langmuir 2026, 42, 21207−21216

light intensity I to heat the water at the bottom to the critical temperature T_c required to induce convection, which is mainly determined by the heat capacity and light intensity. Once $T > T_c$, the fluid instability drives the high-speed convection.

However, the motion of the particles suddenly stops after a period of high-speed convection, which is likely attributed to the disappearance of the vertical temperature difference. The strong convection rapidly mixes the heat, resulting in a decrease in the temperature difference. Meanwhile, the inherent asymmetry of the thermal convection causes the downward flow to be narrow and fast, while the upward flow is wide and slow.[36] Therefore, the number of particles in the upper region decreases rapidly, while the particles in the lower part of the droplet cannot be propelled to supplement the decreased number of particles in time in the upper region. As a result, the particle distribution returns to its initial state. As a result, heat must be reabsorbed to rebuild the temperature difference. During the second cycle, the microspheres moved to the upper part of the droplet again by thermal Marangoni flow and self-thermophoresis, generating a temperature difference sufficient to trigger thermal convection. In general, the fast-motion phase is a self-excited oscillatory convection triggered when the temperature difference reaches a critical point, and it stops when convection dissipates the gradient.

Influence of Light Intensity

We have studied the effect of irradiation intensity on the oscillatory collective behavior. The collective behavior can be altered from self-thermophoresis to oscillatory motion, continuous convection with the increasing of light intensity. As shown in Figure 4a,b and Video S2 (Self-thermophoresis motion under weak light intensity) in the Supporting Information, self-thermophoresis motion is observed in the PVA−PPy solution (0.4 vol % in water) upon weak light intensity (0.2 W/cm^2). Most of the PVA−PPy microspheres move upward away from the light spot below with an average speed of approximately 10 μm/s (Figure 4g). The temperature of the irradiated center is only 26.7 °C, and the temperature difference is insufficient to generate the high-speed convection (Figure 4c). When the light intensity increases to 0.4 W/cm^2, oscillatory behavior can be observed, and its frequency increases with intensity (Figure 4h). Meanwhile, the temperature at the irradiated center (Figure S4 in the Supporting Information) and the maximum oscillation speed increase (Figure S5 in the Supporting Information) with the increasing light intensity. However, the motion of the microspheres becomes continuous with a speed of about 2015 μm/s upon strong irradiation intensity (1.2 W/cm^2), as shown in Figure 4d,e,I and Video S3 (Continuous convection upon strong light intensity) in the Supporting Information, all the microspheres move toward the irradiation center and exhibit the continuous convection motion. The temperature of the irradiated center can reach 41 °C, indicating the strong photothermal effect upon high light intensity (Figure 4f). Note that the thermogravimetric analysis (TGA) reveals that the PVA−PPy microspheres are stable in water before 148 °C (Figure S6 in the Supporting Information), which is far greater than the maximum temperature (41 °C) generated by the photothermal effect. Thus, it can be confidently believed that the strong photothermal effect under high light intensity disrupts the periodic variation of the temperature difference, and the heat generated under high light intensity is sufficient to maintain the temperature gradient required for driving high-speed convection. Therefore, the precise control of the moving direction of PVA−PPy microsphere to maintain the oscillatory motion depends on the appropriate light intensity and static of irradiated condition.

In summary, the oscillatory collective behavior only exists in medium light intensity from about 0.4 to 1 W/cm^2. Therefore, by adjusting the light intensity, the collective behaviors of PVA−PPy microspheres can be tuned from self-thermophoresis to oscillatory motion and to continuous convection. We have analyzed the possible mechanisms of motion behaviors under different light intensities. When the Rayleigh number R_a of the system exceeds the critical value R_{ac}, convection will occur. If the calculated Rayleigh number R_a is less than the critical value R_{ac}, it indicates that the motion is not self-sustaining, and the movement of microspheres will stop. Moreover, when the light intensity I and concentration φ cause the Rayleigh number of the static system to exceed R_{ac}, oscillations can be generated. First of all, we need to clarify the critical condition: the threshold for convective instability in the system, defined by the critical temperature difference ΔT_c, is determined by the critical Rayleigh number R_{ac}:[37]

$$R_a = \frac{g\beta L^3 \Delta T}{\nu\kappa} > R_{ac} \tag{1}$$

$$\Rightarrow \Delta T > \Delta T_c = \frac{R_{ac}\nu\kappa}{g\beta L^3} > R_{ac} \tag{2}$$

Here, β is the solvent thermal expansion coefficient, κ is the solvent thermal diffusivity, L is the system thickness, and ν is the fluid kinematic viscosity. Here, ΔT is the total temperature difference across the droplet thickness L (i.e., $\Delta T = T_{\text{bottom}} - T_{\text{top}}$). ΔT_c is a constant determined by the droplet thickness L and the fluid properties.

Second, establishing the energy balance equation under quasi-steady state conditions, the input power equals the dissipated power:

$$\alpha I\varphi \approx \lambda \Delta T \tag{3}$$

where α is the particle absorption coefficient, and λ is the effective thermal conductivity. When the particles are in a slow-motion phase, heat transfer is dominated by thermal conduction ($\lambda = \lambda_{\text{cond}}$), where λ is small, and heat dissipation is slow. While fast motion is dominated by thermal convection ($\lambda = \lambda_{\text{conv}}$), when λ is large, and heat dissipation is fast.

Third, establishing the condition for oscillations to occur is that the light intensity I must simultaneously satisfy the following two inequalities:

Condition 1: The lower threshold that can trigger oscillatory behavior, such that the oscillatory motion is just enough to initiate. The temperature difference generated at this point must be sufficient to trigger convection:

$$\alpha I\varphi > \lambda_{\text{cond}} \Delta T_c \tag{4}$$

$$\Rightarrow I > I_{c1} = \frac{\lambda_{\text{cond}} \Delta T}{\alpha\varphi} \tag{5}$$

If $I < I_{c1}$, the system will remain in a steady state under low light intensity, leading to the weak thermophoretic motion.

Condition 2: The upper threshold at which particles' motion stops during the burst phase of high-speed convection, where the temperature difference across the system decreases rapidly

https://doi.org/10.1021/acs.langmuir.6c02095
Langmuir 2026, 42, 21207−21216

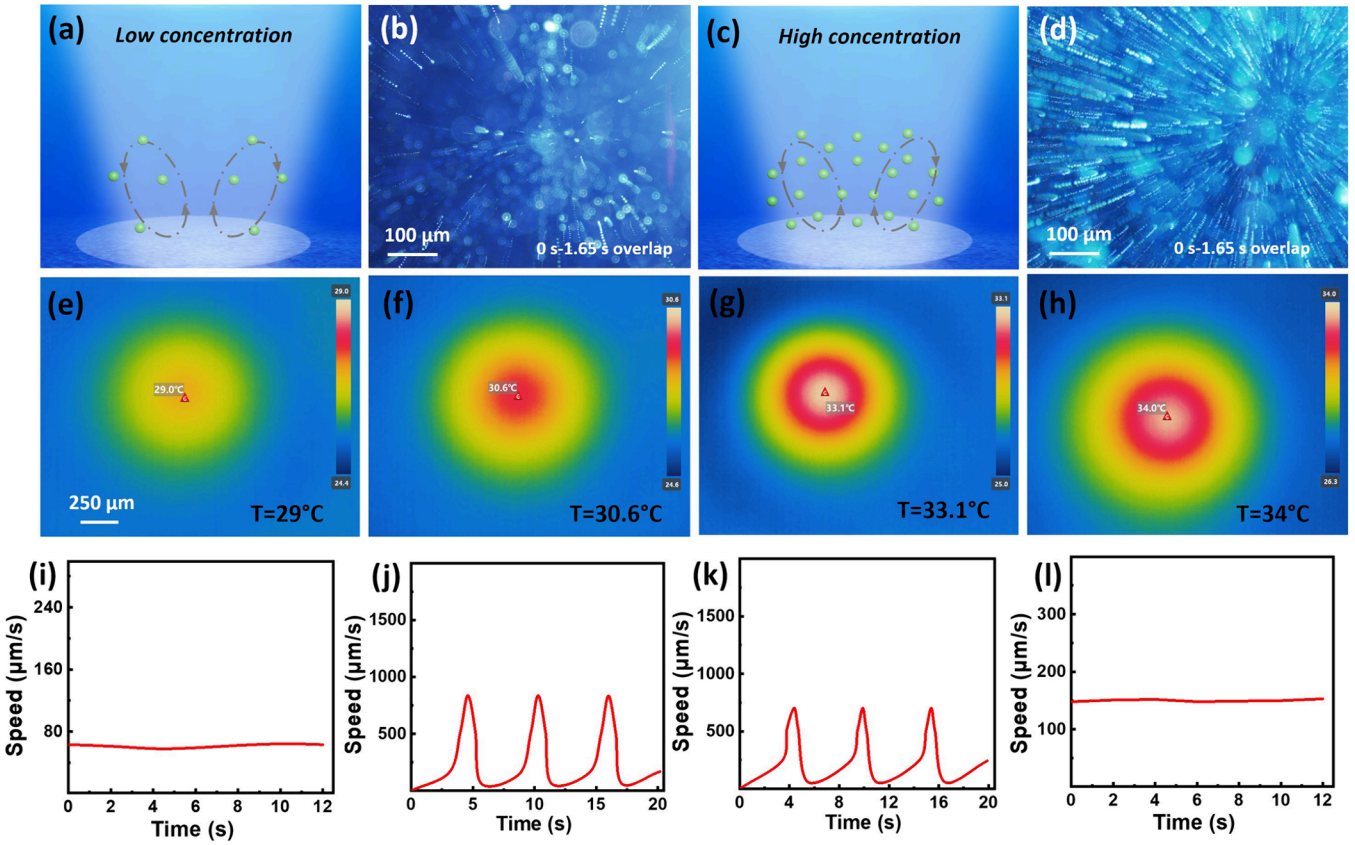

Figure 5. Influence of microspheres' concentration. Schematic illustration and corresponding overlap images showing the continuous motion of PVA−PPy microspheres with (a, b) low concentration (0.04 vol %) and (c, d) high concentration (4 vol %) upon light irradiation. (e−h) Infrared thermal images showing the temperature distribution in the different concentrations of 0.04 vol %, 0.1 vol %, 1.6 vol %, and 4 vol % concentration of PVA−PPy microspheres, respectively. Moving speed vs time of (i) 0.04 vol %, (j) 0.1 vol %, (k) 1.6 vol %, and (l) 4 vol % concentration of PVA−PPy microspheres.

due to the rapid convective flow of particles, becoming insufficient to sustain convection:

$$I < I_{c2} = \frac{\lambda_{conv}\Delta T}{\alpha\varphi} \tag{6}$$

If $I > I_2$, the light intensity is enough to maintain the $R_a > R_{ac}$, and the system enters a steady state of continuous strong convection under high light intensity. In addition, the oscillation period (t_{total}) is influenced by light intensity.

$$t = t_h + t_c \tag{7}$$

t_h is the time required for the particles to slowly convert light-to-heat for the temperature difference to increase from 0 to the critical value that triggers convection. t_c is defined as the time interval between the initiation and the termination of the particle's high-speed convection. Both t_h and t_c decrease with increasing light intensity, leading to a shorter oscillation period and thus a higher frequency. A detailed derivation of the relationship between light intensity and oscillation frequency is provided in Section S6 in the Supporting Information.

Overall, under weak light intensity, the photothermal effect is too weak to reach the threshold required for generating high-speed motion. Within the intensity range where particle oscillations occur, increasing the light intensity accelerates both the build-up and dissipation of the temperature difference, thereby continuously shortening the motion period of each cycle. Under high light intensity, the build-up and dissipation times of the temperature difference approach infinitesimally small values, leading to the continuous motion due to the sustainable temperature gradient. Therefore, the motion behavior of the particles can be regulated by light intensity.

Influence of Micromotors' Concentration

Additionally, the concentration of PVA−PPy microspheres can also affect the motion behaviors, in which the oscillatory collective behavior only exists in medium concentration. As shown in Figure 5a,b and Video S4 (Continuous motion driven by self-thermophoretic motion/thermal Marangoni flow in medium concentration) in the Supporting Information, the overlap CCD images show the trajectory of PVA−PPy microspheres with the low concentration of 0.04 vol % upon medium light irradiation (0.8 W/cm^2), they move toward the irradiation center and then move toward the upper and edge of the droplet to form a continuous motion with the average speed of ∼60 μm/s (Figure 5i). Under sustained and stable light irradiation, the particles will continue to move in this manner without any change in their motion state or velocity.

When the microsphere concentration reaches 0.1 vol %, collective oscillations begins to appear. As shown in Figure 5j, the oscillation frequency and maximum oscillatory speed are 0.175 Hz (Figure S7 in the Supporting Information) and 836 μm/s, respectively. When the concentration increases to 0.4 vol %, both values rise to 0.23 Hz and 2422 μm/s (Figure 2i). However, as the concentration further increases to 1.6 vol %, the oscillation frequency and maximum oscillatory speed decrease to 0.15 Hz and 702 μm/s, respectively (Figure 5k and

https://doi.org/10.1021/acs.langmuir.6c02095
Langmuir 2026, 42, 21207−21216

Figure S8 in the Supporting Information). Therefore, under a fixed light intensity of 0.8 W/cm^2, the oscillation frequency and maximum speed first increase from 0.1 vol % to 0.4 vol % and then decrease from 0.4 vol % to 1.6 vol %. When the concentration is raised to a high value of 4 vol %, the oscillatory motion disappears and is replaced by continuous motion, as shown in Figure 5c,d, and Video S5 (Continuous motion of PVA−PPy microspheres with high concentration) in the Supporting Information. The average speed under this condition is about 150 μm/s (Figure 5l). The infrared thermal images in Figure 5 (e-h) show that the temperature at the irradiated center increases from 26.7 °C (at 0.04 vol %) to 41 °C (at 4 vol %), indicating that the photothermal effect becomes stronger with increasing concentration. Notably, for either very low or very high concentrations, the motion cannot be switched to oscillatory behavior by adjusting the light intensity. Although the moving speed increases with higher light intensity (Figure S9 in the Supporting Information), it remains much lower than the maximum speed achieved during oscillatory motion.

In the analysis above, the influence of colloidal particle concentration on the solvent properties has been neglected. In reality, colloidal particles can modify the buoyancy effect and also affect the solution's viscosity (especially at higher concentrations). These effects can be accounted for by defining an effective Rayleigh number (see Section S5 in the Supporting Information for details).[38] Therefore, particles can exhibit the following three situations at different concentrations.

(1) Low concentration particles: Since φ appears in the denominator as $1/\varphi$, the resistance to flow initiation becomes extremely large. Physical interpretation: a low concentration of absorbing particles cannot generate enough heat to reach the required temperature difference unless the light intensity is extremely high. Consequently, the colloidal particles can only exhibit thermophoretic motion/thermal Marangoni flow at the gas−liquid interface (due to the higher temperature in the central region) may induce only weak convection of the particles. In this case, the flow remains steady because Marangoni flow does not require a specific threshold to begin and can be maintained under a constant thermal gradient.

(2) Medium concentration particles: When φ is moderate, the particles can generate a sufficient temperature difference, so that $I > I_{c1}$. When φ is very small, convection can effectively transport the particles, thereby making I_{c2} very high and satisfying $I < I_{c2}$. Together, these conditions create a concentration window within which oscillations can occur.

(3) High concentration particles: When $1/\varphi$ becomes smaller and the experimental light intensity $I > I_{c1}$, convection will initiate due to the sufficient supply of absorbing particles. Consequently, the convection cannot be stopped and persists as a continuous flow. However, the speed of continuous motion is slow, because colloidal particles are too dense and too viscous. Most of the energy generated by thermal buoyancy is consumed to overcome the combined effects of increased effective gravity and viscosity within the colloidal suspension. The remaining energy is only sufficient to sustain slow motion. This can be understood from the following scaling relation for velocity, which is derived from the effective Rayleigh number for the colloidal solution:

$$U \sim \frac{\kappa}{L}\sqrt{R_{aff} - R_{ac}} \tag{8}$$

This equation provides a qualitative expression for the convective velocity. Moreover, concentration also has some effect on the oscillation frequency. Initially, as the particle concentration increases, the oscillation frequency increases slightly. This is because a higher particle concentration absorbs light faster, so it takes less time to build the temperature difference needed for high-speed convection. According to eqs 10 and 11 in the Supporting Information, both t_h and t_c decrease in this case. However, when the concentration becomes too high, the situation is completely different. According to Einstein's viscosity equation, the viscosity of the droplet increases with the increasing of microparticles concentration.[39] Therefore, the negative effects of viscosity become more and more significant as concentration increases. The thermal buoyancy is consumed by this resistance, making the motion slower in both the slow and fast phases, and the oscillation frequency decreases significantly. Additionally, the influence of PPy content in PVA−PPy microsphere on the oscillation frequency has been also investigated. As shown in Figure S10 in the Supporting Information. A higher PPy content enhances the absorption coefficient α, shortens the heating time t_h, and thus increases the oscillation frequency.

CONCLUSIONS

In conclusion, a unique oscillatory collective behavior of the photothermal PVA−PPy-based micromotors is demonstrated. These micromotors can be synthesized via a one-step emulsion method. Under illumination, two motion modes of oscillatory collective behavior are observed. Slow-motion propelled by thermophoresis and thermocapillary flow, followed by a fast motion phase driven by thermal convection. The system repeatedly switches between these two states, resulting in a periodic oscillatory motion, and the oscillation frequency can be modulated by varying the light intensity and the concentration of the micromotors. Furthermore, this phenomenon occurs only within a specific range of both light intensity and particle concentration, and outside this range, the motion becomes single. These findings provide a novel strategy for achieving and controlling collective dynamics in synthetic active matter and open new avenues for designing more complex, coupled oscillatory systems in microrobotics and biomimetic applications.

EXPERIMENTAL SECTION

Materials

Liquid paraffin was obtained from Adamas (Shanghai, China). Span 80, pyrrole, ferric chloride ($FeCl_3$), and poly(vinyl alcohol) (PVA) were purchased from Aladdin Reagent (Shanghai, China).

Preparation of PVA−PPy microspheres

0.75 g of PVA was first dissolved in 10 mL of deionized water, then the solution was kept at 60 °C and agitated vigorously for 30 min to ensure complete dissolution. 0.63 g of $FeCl_3$ was then added to the solution and stirred for 30 min. The mixture solution was placed in a 5 °C water bath, and 69 μL of pyrrole was then added into this

https://doi.org/10.1021/acs.langmuir.6c02095
Langmuir 2026, 42, 21207−21216

solution. Polypyrene dispersion was obtained after a 24 h reaction. One ml of the polypyrene dispersion was added to 10 mL of liquid paraffin containing 0.5 g Span 80 and stirred for 20 min. Acetone was then added to the solution to remove water from the resulting microparticles. After filtration and drying, PVA−PPy microspheres were finally dispersed in 10 mL of water. The low, medium and high concentration particles is 0.04 vol %, 0.4 vol %, and 4 vol %, respectively. Unless otherwise mentioned, the PPy content inside the microsphere is 8.2 wt %.

Characterizations

The scanning electron microscopy (SEM) experiment was carried out on a Carl Zeiss Supra 55 scanning electron microscopes with an energy-dispersive X-ray (EDX) analysis attachment. The SEM sample was prepared by drop-casting the solutions containing the PVA−PPy microspheres on a cover glass. Solvent was allowed to evaporate before SEM examination. A 6 nm thick gold layer was sputtered on the surface of PVA−PPy microspheres before SEM observation. The locomotion of microspheres was recorded and captured by the Nikon eclipse 80i microscope. The observation plane is set in the middle-to-upper region of the droplet, such that microspheres become clearer as they approach the focal plane and become blurred as they move away from it. The movement of the micromotor under light irradiation was realized by applying an X-Cite 120Q (Excelitas technologies) light source with tuning on and off, and different intensities and incident angles 1 cm away from the micromotors. We analyzed the captured videos using the PhysVis software to obtain the trajectory and speed of PVA−PPy microspheres. UV-vis-NIR measurements were carried out on a PerkinElmer Lambda 750 spectrophotometer. FTIR measurement was carried out on a Hyperion spectrophotometer (Bruker). The infrared thermal images were obtained by utilizing the FLIR-A300 camera (FLIR Systems Inc.).

■ ASSOCIATED CONTENT

Supporting Information

The Supporting Information is available free of charge at https://pubs.acs.org/doi/10.1021/acs.langmuir.6c02095.

FTIR spectrum of PVA−PPy microspheres; control experiment eliminating the liquid−air interface; high-speed motion without interface; temperature of irradiated center under different light intensity; maximum oscillation speed under various light intensities; TGA curve; oscillation frequency as a function of microsphere concentration; maximum speed with different concentration; moving speed at high concentration and low concentration under different light intensity; oscillation frequency as a function of PPy content (PDF)

Video S1: video showing collective oscillation (MP4)

Video S2: video showing self-thermophoresis (MP4)

Video S3: video showing continuous convection (MP4)

Video S4: video showing continuous motion at low concentrations (MP4)

Video S5: video showing continuous motion at high concentrations (MP4)

■ AUTHOR INFORMATION

Corresponding Authors

Dan Wang − *School of Chemistry and Chemical Engineering, Anhui University of Technology, Ma'anshan, Anhui 243032, China;* orcid.org/0009-0009-2452-5809; Email: wangdan@ahut.edu.cn

Bin Dong − *Institute of Functional Nano and Soft Materials (FUNSOM), Jiangsu Key Laboratory for Carbon-Based Functional Materials and Devices, State and Local Joint Engineering Laboratory for Novel Functional Polymeric Materials, Soochow University, Suzhou, Jiangsu 215123, China;* orcid.org/0000-0001-5681-372X; Email: bdong@suda.edu.cn

Mingcheng Yang − *Beijing National Laboratory for Condensed Matter Physics and Laboratory of Soft Matter Physics, Institute of Physics, Chinese Academy of Sciences, Beijing 100190, China*; Email: mcyang@iphy.ac.cn

Authors

Yuhang Zhang − *School of Chemistry and Chemical Engineering, Anhui University of Technology, Ma'anshan, Anhui 243032, China*

Mingtong Li − *Physical Intelligence Department, Max Planck Institute for Intelligent Systems, 70569 Stuttgart, Germany*

Youyi Xia − *School of Chemistry and Chemical Engineering, Anhui University of Technology, Ma'anshan, Anhui 243032, China;* orcid.org/0000-0002-5258-7128

Ling Jin − *School of Chemistry and Chemical Engineering, Anhui University of Technology, Ma'anshan, Anhui 243032, China;* orcid.org/0000-0002-6960-5150

BingBing Wang − *School of Chemistry and Chemical Engineering, Anhui University of Technology, Ma'anshan, Anhui 243032, China;* orcid.org/0009-0009-6251-6348

Hong Gao − *School of Chemistry and Chemical Engineering, Anhui University of Technology, Ma'anshan, Anhui 243032, China;* orcid.org/0000-0002-5173-5547

Complete contact information is available at: https://pubs.acs.org/10.1021/acs.langmuir.6c02095

Author Contributions

The manuscript was written through contributions of all authors. All authors have given approval to the final version of the manuscript.

Notes

The authors declare no competing financial interest.

■ ACKNOWLEDGMENTS

This work was supported by National Natural Science Foundation of China (Grant No. 52403311), Anhui Provincial Universities Natural Science Research Project (nos. KJ2021A0398 and 2024AH050167), Anhui University Outstanding Youth Research Project (no. 2023AH020018).

■ REFERENCES

(1) Goldbeter, A. Computational approaches to cellular rhythms. *Nature* **2002**, *420*, 238−245.

(2) Fu, F.; Shang, L.; Chen, Z.; Yu, Y.; Zhao, Y. Bioinspired living structural color hydrogels. *Sci. Robot.* **2018**, *3*, No. eaar8580.

(3) Brandman, O.; Meyer, T. Feedback loops shape cellular signals in space and time. *Science* **2008**, *322*, 390−395.

(4) Wang, D.; Zhao, G.; Chen, C.; Zhang, H.; Duan, R.; Zhang, D.; Li, M.; Dong, B. One-step fabrication of dual optically/magnetically modulated walnut-like micromotor. *Langmuir* **2019**, *35*, 2801−2807.

(5) Tong, J.; Wang, D.; Liu, Y.; Lou, X.; Jiang, J.; Dong, B.; Dong, R.; Yang, M. Bioinspired micro/nanomotor with visible light energy-dependent forward, reverse, reciprocating, and spinning schooling motion. *Proc. Natl. Acad. Sci. U S A* **2021**, *118*, No. e2104481118.

(6) Chen, C.; Mou, F.; Xu, L.; Wang, S.; Guan, J.; Feng, Z.; Wang, Q.; Kong, L.; Li, W.; Wang, J.; Zhang, Q. Light-steered isotropic semiconductor micromotors. *Adv. Mater.* **2017**, *29*, 1603374.

(7) Wang, J.; Wu, H.; Zhu, X.; Zwolsman, R.; Hofstraat, S. R. J.; Li, Y.; Luo, Y.; Joosten, R. R. M.; Friedrich, H.; Cao, S.; Abdelmohsen,

L.; Shao, J.; van Hest, J. C. M. Ultrafast light-activated polymeric nanomotors. *Nat. Commun.* **2024**, *15*, 4878.
(8) Gao, C.; Feng, Y.; Liu, S.; Chen, B.; Ding, M.; Du, D.; Zhang, W.; Wilson, D. A.; Tu, Y.; Peng, F. Light-driven artificial cell micromotors for degenerative knee osteoarthritis. *Adv. Mater.* **2025**, *37*, No. e2416349.
(9) Solovev, A. A.; Sanchez, S.; Pumera, M.; Mei, Y. F.; Schmidt, O. G. Magnetic control of tubular catalytic microbots for the transport, assembly, and delivery of micro-objects. *Adv. Funct. Mater.* **2010**, *20*, 2430−2435.
(10) Wu, Y.; Yakov, S.; Fu, A.; Yossifon, G. A magnetically and electrically powered hybrid micromotor in conductive solutions: Synergistic propulsion effects and label-free cargo transport and sensing. *Adv. Sci.* **2023**, *10*, No. e2204931.
(11) Liu, M.; Wang, Y.; Kuai, Y.; Cong, J.; Xu, Y.; Piao, H. G.; Pan, L.; Liu, Y. Magnetically powered shape-transformable liquid metal micromotors. *Small* **2019**, *15*, 1905446.
(12) Sharma, R.; Velev, O. D. Remote steering of self-propelling microcircuits by modulated electric field. *Adv. Funct. Mater.* **2015**, *25*, 5512−5519.
(13) Loget, G.; Kuhn, A. Electric field-induced chemical locomotion of conducting objects. *Nat. Commun.* **2011**, *2*, 535.
(14) Xu, X.; Liu, C.; Kim, K.; Fan, D. L. Electric-driven rotation of silicon nanowires and silicon nanowire motors. *Adv. Funct. Mater.* **2014**, *24*, 4843−4850.
(15) Athanassiadis, A. G.; Ma, Z.; Moreno-Gomez, N.; Melde, K.; Choi, E.; Goyal, R.; Fischer, P. Ultrasound-responsive systems as components for smart materials. *Chem. Rev.* **2022**, *122*, 5165−5208.
(16) Jiang, Z.; Wei, C.; Cai, S.; Fu, Q. Ultrasound-propelled nanomotors enable activatable Near-Infrared-II fluorescence imaging-guided synergistic oxygen-independent and oxygen-dependent sonodynamic therapy of atherosclerosis. *Adv. Funct. Mater.* **2025**, *35*, 2503885.
(17) Su, Y.; Ge, Y.; Liu, L.; Zhang, L.; Liu, M.; Sun, Y.; Zhang, H.; Dong, B. Motion-based pH sensing based on the cartridge-case-like micromotor. *ACS Appl. Mater. Interfaces* **2016**, *8*, 4250−4257.
(18) Soler, L.; Magdanz, V.; Fomin, V. M.; Sanchez, S.; Schmidt, O. G. Self-propelled micromotors for cleaning polluted water. *ACS Nano* **2013**, *7*, 9611−9620.
(19) Zhang, D.; Wang, D.; Li, J.; Xu, X.; Zhang, H.; Duan, R.; Song, B.; Zhang, D.; Dong, B. One-step synthesis of PCL/Mg Janus micromotor for precious metal ion sensing, removal and recycling. *J. Mater. Sci.* **2019**, *54* (9), 7322−7332.
(20) Nakata, S.; Nomura, M.; Yamamoto, H.; Izumi, S.; Suematsu, N. J.; Ikura, Y.; Amemiya, T. Periodic oscillatory motion of a self-propelled motor driven by decomposition of H_2O by Catalase. *Angew. Chem., Int. Ed.* **2017**, *56*, 861−864.
(21) Sharma, R.; Chang, S. T.; Velev, O. D. Gel-based self-propelling particles get programmed to dance. *Langmuir* **2012**, *28*, 10128−10135.
(22) Nakata, S.; Murakami, M. Self-motion of a camphor disk on an aqueous phase depending on the alkyl chain length of sulfate surfactants. *Langmuir* **2010**, *26*, 2414−2417.
(23) Suematsu, N. J.; Nakata, S. Evolution of self-propelled objects: From the viewpoint of nonlinear science. *Chem.—Eur. J.* **2018**, *24*, 6308−6324.
(24) Ibele, M. E.; Lammert, P. E.; Crespi, V. H.; Sen, A. Emergent, collective oscillations of self-mobile particles and patterned surfaces under redox conditions. *ACS Nano* **2010**, *4*, 4845−4851.
(25) Zhou, C.; Chen, X.; Han, Z.; Wang, W. Photochemically excited, pulsating janus colloidal motors of tunable dynamics. *ACS Nano* **2019**, *13*, 4064−4072.
(26) Chen, X.; Zhou, C.; Peng, Y.; Wang, Q.; Wang, W. Temporal light modulation of photochemically active, oscillating micromotors: Dark pulses, mode switching, and controlled clustering. *ACS Appl. Mater. Interfaces* **2020**, *12*, 11843−11851.
(27) Gao, C.; Feng, Y.; Liu, S.; Fu, D.; Chen, B.; Du, D.; Zhang, W.; Gao, Z.; Yang, H.; Wilson, D. A.; Tu, Y.; Peng, F. Water-powered Cu@MoS_2 micromotor swarm for a collaborative oscillation of living cells. *Matter* **2023**, *6*, 3956−3974.
(28) Altemose, A.; Sanchez-Farran, M. A.; Duan, W.; Schulz, S.; Borhan, A.; Crespi, V. H.; Sen, A. Chemically controlled spatiotemporal oscillations of colloidal assemblies. *Angew. Chem., Int. Ed.* **2017**, *56*, 7817−7821.
(29) Petrov, V.; Gáspár, V.; Masere, J.; Showalter, K. Controlling chaos in the Belousov—Zhabotinsky reaction. *Nature* **1993**, *361*, 240−243.
(30) Xuan, M.; Wu, Z.; Shao, J.; Dai, L.; Si, T.; He, Q. Near infrared light-powered janus mesoporous silica nanoparticle motors. *J. Am. Chem. Soc.* **2016**, *138*, 6492−6497.
(31) Jiang, H. R.; Yoshinaga, N.; Sano, M. Active motion of a Janus particle by self-thermophoresis in a defocused laser beam. *Phys. Rev. Lett.* **2010**, *105*, 268302.
(32) Xu, T.; Gao, W.; Xu, L. P.; Zhang, X.; Wang, S. Fuel-free synthetic micro-/nanomachines. *Adv. Mater.* **2017**, *29*, 1603250.
(33) Ichikawa, M.; Takabatake, F.; Miura, K.; Iwaki, T.; Magome, N.; Yoshikawa, K. Controlling negative and positive photothermal migration of centimeter-sized droplets. *Phys. Rev. E* **2013**, *88*, 012403.
(34) Zhang, N. Q.; Li, C. X.; Meng, C.; Yu, P.; Chen, D.; Zhong, M. C. Optothermal oscillation of hollow microparticles near a droplet surface. *Appl. Opt.* **2025**, *64*, 4142−4147.
(35) Qian, Y.; Neale, S. L.; Marsh, J. H. Microparticle manipulation using laser-induced thermophoresis and thermal convection flow. *Sci. Rep.* **2020**, *10*, 19169.
(36) Busse, F. H. Non-linear properties of thermal convection. *Rep. Prog. Phys.* **1978**, *41*, 1929−1967.
(37) Sherman, M. Onset of thermal instability in a horizontal circular cylinder. *Phys. Fluids* **1966**, *9*, 2095−2101.
(38) Ryskin, A.; Pleiner, H. Thermal convection in colloidal suspensions with negative separation ratio. *Phys. Rev. E* **2005**, *71*, 056303.
(39) Einstein, A. A New Determination of Molecular Dimensions. *Ann. Phys.* **1906**, *324*, 289.

https://doi.org/10.1021/acs.langmuir.6c02095
Langmuir 2026, 42, 21207−21216